Possible chiral topological superconductivity in CrO_2 bilayers

Xu Dou, Kangjun Seo, and Bruno Uchoa*
Department of Physics and Astronomy, University of Oklahoma, Norman, Oklahoma 73069, USA

(Received 4 April 2018; revised manuscript received 3 November 2018; published 4 March 2019)

We address the possible emergence of spin triplet superconductivity in CrO_2 bilayers, which are half-metals with fully spin-polarized conducting bands. Starting from a lattice model, we show that chiral $p+ip$ states compete with nonchiral p-wave ones. At large doping, the $p+ip$ channel has a sequence of topological phase transitions that can be tuned by gating effects and interaction strength. Among several phases, we find chiral topological phases having a single Majorana mode at the edge. We show that different topological superconducting phases could spontaneously emerge in the vicinity of the van Hove singularities of the band.

DOI: 10.1103/PhysRevB.99.104503

I. INTRODUCTION

Half-metals such as CrO_2 [1,2] are promising materials for the prospect of emergent topological superconductivity (TSC). By having a metallic Fermi surface with a single spin, they raise the possibility of chiral superconductivity in the triplet channel [3], which is believed to occur only in a handful of systems such as Sr_2RuO_4 [4], which may have a spinful triplet state, UPt_3, and some heavy fermion superconductors [5,6]. A distinctive property of spin triplet chiral topological superconductivity is the presence of Majorana fermions propagating at the edges [7–12] and half-flux quantum vortices [13,14] that can trap Majorana modes [15,16]. Majorana edge states were predicted to exist in different heterostructures with strong spin-orbit coupling [17–22] and may have been recently observed in an anomalous Hall insulator-superconductor structure [23,24].

In its most common form, CrO_2 is a three-dimensional bulk material with a rutile structure [25,26]. It was recently suggested [27] that CrO_2/TiO_2 heterostructures have fully spin-polarized conduction bands over a wide energy window around the Fermi level, and behave effectively as a two-dimensional (2D) crystal. In its simplest 2D form, CrO_2 will form a bilayer. It is natural to ask if this material could spontaneously develop 2D chiral topological superconducting phases and host Majorana fermions [17].

We start from a lattice model for a single CrO_2 bilayer to address the formation of spin triplet pairs either with p-wave or p_x+ip_y symmetry, which leads to a fully gapped state. Due to the strong anisotropy of the gap, the superconducting order has a line of quantum critical points as a function of both doping and coupling strength. In the $p+ip$ state, we show that the system has an exotic sequence of topological phase transitions that could be tuned with gating effects. Different nontrivial topological phases may occur in the vicinity of van Hove singularities of the band, where the density of states (DOS) diverges, allowing the possibility for both conventional and purely electronic mechanisms. We suggest that this system may provide an experimental realization of intrinsic 2D chiral topological superconductivity in the triplet channel.

II. LATTICE MODEL

In a bilayer system, the Cr atoms form two interpenetrating square sublattices, A and B, each one sitting on a different layer. From above, the Cr atoms are arranged in a checkerboard pattern, as shown in Fig. 1. Each site on sublattice A (B) has two orbitals with d_{xy} and d_{xz} (d_{yz}) symmetry. Nearest-neighbor (NN) hopping between a d_{xy} orbital in sublattice B with a d_{xz} orbital in sublattice A has an amplitude t_1 along the $(1,\bar{1})$ direction and zero along the (1,1) direction by symmetry. In the same way, NN hopping between a d_{xy} orbital in sublattice A and with a d_{yz} orbital in B has an amplitude t_2 along the (1,1) direction and zero along the other diagonal in the xy plane. Intraorbital NN hopping is finite between d_{xy} orbitals (t_3) but zero between d_{xz} and d_{yz} orbitals (t_4), which are orthogonal to each other. Among next-nearest neighbors (NNN), the dominant processes are described by intraorbital hoppings t_j^α, with $\alpha = xy, xz$ for sites in sublattice $j = A$ and $\alpha = xy, yz$ for B sites.

The Hamiltonian can be described in a four-component basis $\Psi = (\psi_{A,xy}, \psi_{A,xz}, \psi_{B,xy}, \psi_{B,yz})$. In momentum space, $\mathcal{H}_0 = \sum_{\mathbf{q}} \Psi_{\mathbf{q}}^\dagger h(\mathbf{q}) \Psi_{\mathbf{q}}$, with [27]

$$h(\mathbf{q}) = \begin{pmatrix} h_A & h_{AB} \\ h_{AB}^\dagger & h_B \end{pmatrix}, \tag{1}$$

where

$$h_A = \begin{pmatrix} \epsilon_A^{xy}(\mathbf{q}) & 0 \\ 0 & \epsilon_A^{xz}(\mathbf{q}) \end{pmatrix}, \quad h_B = \begin{pmatrix} \epsilon_B^{xy}(\mathbf{q}) & 0 \\ 0 & \epsilon_B^{yz}(\mathbf{q}) \end{pmatrix}. \tag{2}$$

The diagonal terms incorporate NNN hopping processes, where $\epsilon_j^\alpha(\mathbf{q}) = E_j^\alpha + 4t_j^\alpha \cos q_x \cos q_y$, with E_j^α a local potential on orbital α in sublattice j and $q_{x,y} = \frac{1}{2}(k_x \mp k_y)$ the momentum along the two diagonal directions of the crystal. The off-diagonal terms in (1) describe the NN hopping terms illustrated in Figs. 1(a) and 1(b),

$$h_{AB} = \begin{pmatrix} -2t_3 \sum_{v=x,y} \cos q_v & 2it_1 \sin q_y \\ 2it_2 \sin q_x & -2t_4 \sum_{v=x,y} \cos q_v \end{pmatrix}, \tag{3}$$

where $t_4 = 0$ in the absence of spin-orbit coupling.

*uchoa@ou.edu

 ©2019 American Physical Society

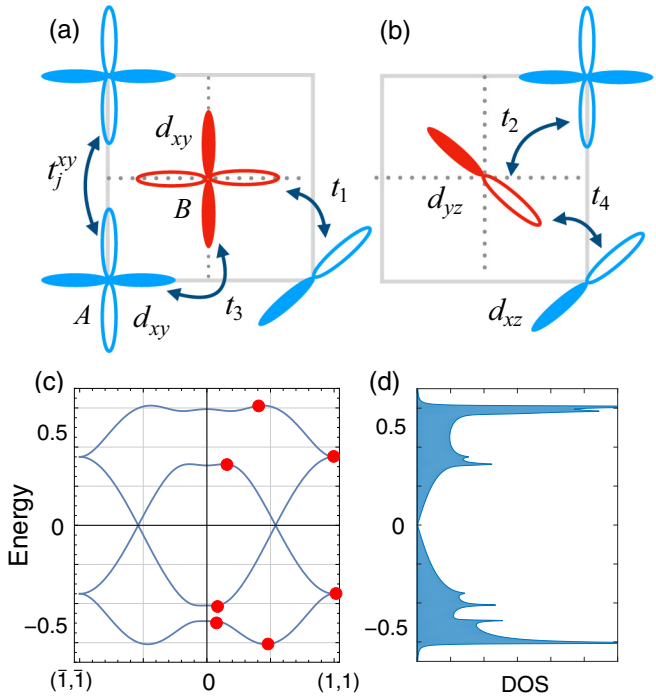

FIG. 1. Top: Lattice of a CrO_2 bilayer, with d_{xy} and d_{xz} (d_{yz}) orbitals in sublattice A (***B***). The blue orbitals sit in the top layer (A sites), and red orbitals in the lower one (B sites). Hopping energies are indicated by t_j^α for intraorbital hopping between next-nearest sites, with $\alpha = xy, xz$ for $j = A$ and $\alpha = xy, yz$ for $j = B$, and t_i ($i = 1, 2, 3, 4$) for nearest-neighbor hopping. (c) Energy spectrum of the lattice model along the diagonal (1,1) direction. Energy axes in eV units. Red dots indicate the location of van Hove singularities, where the DOS (d) diverges logarithmically.

The energy spectrum is shown in Fig. 1(c), and has two sets of Dirac points along the (1,1) and $(1, \bar{1})$ directions, respectively. Enforcing the symmetries of the 2D lattice, namely rotoinversion S_4 symmetry and mirror symmetry M at the diagonal directions of the unit cell, we adopt $t_1 = -t_2 \equiv t \sim 0.3$ eV as the leading energy scale, and the set of parameters $t_3 \sim t/30$, $t_j^{xy} = -t_A^{xz} = -t_B^{yz} \sim t/3$, and $E_j^{xy} = -E_A^{xz} = -E_B^{yz} \sim t/6$. We also use $t_4 \sim it/8$, following *ab initio* results [27,28]. The four-band model breaks down near the edge of the band, where states may hybridize with high-energy bands. We also assume that the bands are spinless. The resulting band structure has several van Hove singularities at the saddle points, where the density of states (DOS) diverges logarithmically, as depicted in Fig. 1(d). In the vicinity of those points (red dots), the system can be unstable towards superconductivity.

III. PAIRING HAMILTONIAN

For spinless fermions, superconductivity is allowed only in the triplet channel. The wave function of the Cooper pairs is antisymmetric under inversion, and hence only states with odd angular momentum are allowed. When electrons pair across the center of the Brillouin zone, the lowest symmetry is in the p-wave channel, which can be induced by NN pairing. f-wave pairing may be induced with NNN pairing only. This channel is subdominant and will not be addressed. We consider the possible instabilities of the lattice model both in the p-wave and in the chiral $p + ip$ state, which can produce a full gap. A conclusive assessment of the stability of those states requires taking fluctuations into account [29–31], which will be considered elsewhere.

For NN sites, the effective interaction term has the form

$$\mathcal{H}_{\rm int} = -\frac{1}{2}\sum_{\mathbf{r}\in \rm NN} g^{\alpha\beta}\hat{n}_{i,\alpha}(\mathbf{r}_i)\hat{n}_{j,\beta}(\mathbf{r}_j), \tag{4}$$

where $\hat{n}_{i,\alpha} = \psi^\dagger_{i,\alpha}\psi_{i,\alpha}$ is the density operator in orbital α on sublattice $i = A, B$, $g^{\alpha\alpha} \equiv g_1 > 0$ is the intraorbital coupling, and $g^{xy,yz} = g^{xz,xy} \equiv g_2 > 0$ is the coupling in the interorbital channel. The $p + ip$ pairing follows from the ansatz on the lattice $\Delta^{\alpha\beta}(\delta_n) = g^{\alpha\beta}\langle\psi_{A,\alpha}(\mathbf{r})\psi_{B,\beta}(\mathbf{r}+\vec{\delta}_n)\rangle \equiv \Delta^{\alpha\beta}e^{i\frac{\pi}{2}n}$, where $\vec{\delta}_{1,3} = \pm\frac{a}{2}(\hat{x}+\hat{y})$ and $\vec{\delta}_{2,4} = \pm\frac{a}{2}(\hat{x}-\hat{y})$ describe the four NN vectors, with a the lattice constant. For p-wave pairing, we use the ansatz $\Delta^{\alpha\beta}(\pm\delta_{1,2}) \equiv \pm\Delta^{\alpha\beta}$.

Defining $\Delta^{\alpha\alpha} \equiv \Delta_1$ and $\Delta^{\alpha\beta} \equiv \Delta_2$ for intraorbital and interorbital pairing. respectively, the order parameter in momentum space $\Delta_i^C(\mathbf{q}) = \Delta_i^C(\sin q_y + i\sin q_x)$ has chiral $p_x + ip_y$ symmetry, with $i = 1, 2$ and $q_{x,y}$ defined as above in Eq. (3). In the nonchiral state, $\Delta_i^p(\mathbf{q}) = \Delta_i^p(\sin q_y + \sin q_x)$ has p_x symmetry [32]. At the mean-field level, Hamiltonian (1) and (4) result in the Bogoliubov–de Gennes (BdG) Hamiltonian $\mathcal{H}_{\rm BdG} = \sum_{\mathbf{k}\in BZ}\Phi^\dagger_{\mathbf{q}}h_{\rm BdG}(\mathbf{q})\Phi_{\mathbf{q}}$ with $\Phi_{\mathbf{q}} = (\Psi_{\mathbf{q}}, \Psi^\dagger_{-\mathbf{q}})$, which has the form

$$h_{\rm BdG}(\mathbf{q}) = \begin{pmatrix} h(\mathbf{q}) & \hat{\Delta}(\mathbf{q}) \\ \hat{\Delta}^\dagger(\mathbf{q}) & -h^T(-\mathbf{q}) \end{pmatrix}, \tag{5}$$

where

$$\hat{\Delta}(\mathbf{q}) = \begin{pmatrix} 0 & \Delta_1(\mathbf{q})\mathbf{1} + \Delta_2(\mathbf{q})\sigma_x \\ \Delta_1(\mathbf{q})\mathbf{1} + \Delta_2(\mathbf{q})\sigma_x & 0 \end{pmatrix} \tag{6}$$

is the pairing matrix, with σ_x a Pauli matrix in the orbital space. Minimization of the free energy $\mathcal{F}(\Delta_1, \Delta_2) = -T\,\mathrm{tr}\sum_{\mathbf{k}}\ln e^{-h_{\rm BdG}(\mathbf{k})/T} + \sum_{i=1,2}|\Delta_i|^2/g_i$ for a fixed chemical potential μ gives the zero temperature ($T = 0$) phase diagram shown in Figs. 2(a) and 2(b) as a function of the couplings g_1 and g_2. The two leading instabilities in the p-wave and chiral $p + ip$ states compete with each other and are addressed below.

A. *p*-wave phase

The vertical line in Fig. 2(a) describes a quantum phase transition at $g_1 = \tilde{g}_{1c}(\mu)$ separating the normal phase (N) from the intraorbital p_x state (pSC I). At $g_2 = \tilde{g}_{2,c}(\mu)$ (dashed line) the system has a first-order phase transition towards an interorbital p-wave state (pSC II). Due to the anisotropy of the p-wave gap, the curve $g = \tilde{g}_{1c}(\mu)$ depicted in Fig. 3(a) describes a line of quantum critical points with power-law scaling [33]. The intraorbital channel ($\Delta_1^p \neq 0$) dominates over the interorbital one for all values of μ. At the mean-field level, it is also the leading instability in the weak-coupling regime of the problem (which we define below), and subleading to the $p + ip$ state in the strong-coupling sector, as indicated in Fig. 3(a).

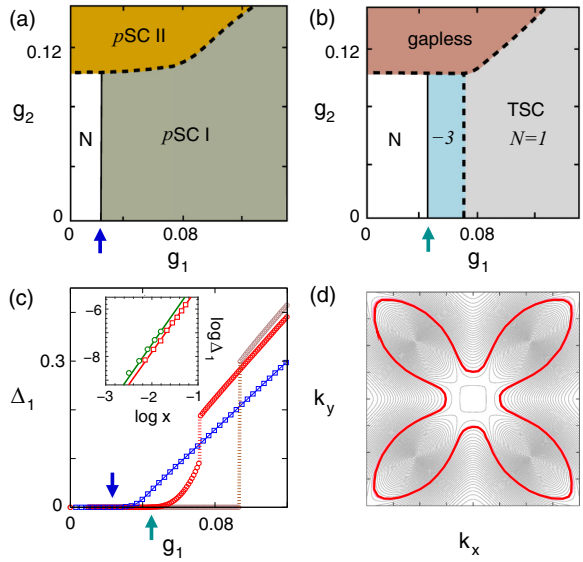

FIG. 2. Phase diagram for (a) p-wave and (b) $p+ip$ state for intraorbital (g_1) and interorbital (g_2) couplings at $\mu = 4t/3 = 0.4$ eV. g_1 and g_2 in eV units. Green area: Intraorbital p-wave (pSC I) for $g > \tilde{g}_{1c}(\mu)$. Yellow: Interorbital p-wave (pSC II). Gray area: Strong-coupling topological phase (TSC) with Chern number $\mathcal{N} = 1$. Light blue: Gapped weak-coupling one ($\bar{g}_{1c} < g < g_{1c}$) with $\mathcal{N} = -3$ [see Fig. 3(b)]. Light red: Gapless $p+ip$, which is topologically trivial. Dashed lines: First-order phase transitions. Solid black lines: Second-order transition (blue and green arrows). (c) Scaling of Δ_1 vs g_1. Red and brown circles: $p+ip$ for $\mu = 0.4$, and 0, respectively. Blue square: p-wave for $\mu = 0.4$ eV. Green and blue arrows: Critical coupling $\bar{g}_{1c} \approx t/7 = 0.045$ eV and $\tilde{g}_{1c} \approx t/12 = 0.025$ eV, respectively, for $\mu = 0.4$ eV. Inset: Δ_1^C vs $\log x$, with $x = (1 - \bar{g}_{1c}/g)$, showing power-law scaling in the chiral phase near $\bar{g}_{1c}(\mu)$. Green dots: $\mu = 0.3$ eV. Red: $\mu = 0.4$ eV. (d) Brillouin zone. Red line: Anisotropic Fermi surface at $\mu = 0.33$ eV.

B. $p+ip$ phase

The interorbital channel g_2 may lead to gapless chiral $p+ip$ superconductivity ($\Delta_2^C \neq 0$) shown in the red region, which is topologically trivial [Fig. 2(a)]. This state dominates over the interorbital pSC II phase, shown in Fig. 2(b). The dashed line around the gapless phase in Fig. 2(b) describes a first-order phase transition and sets the boundary of the gapless $p+ip$ phase with the others at $g_2 = g_{2c}(\mu)$. The intraorbital $p+ip$ pairing state ($\Delta_1^C \neq 0$), on the other hand, is fully gapped and can be topological.

The gapped state has multiple minima that compete. The dashed vertical line in Fig. 2(b) indicates a first-order phase transition between the weak- and strong-coupling topological phases (TSC) at $g_1 = g_{1c}(\mu)$. At this coupling, the superconducting order parameter Δ_1^C jumps [see Fig. 2(c)] and different gapped phases with distinct topological numbers coexist. The resulting gap is very anisotropic around the Fermi surface [Fig. 2(d)]. In the weak-coupling phase $\bar{g}_{1c}(\mu) < g < g_{1c}(\mu)$ shown in the light blue region in Fig. 2(b), the intraorbital chiral gap Δ_1^C scales as a power law with the coupling for fixed μ,

$$\Delta_1^C(g_1) \propto (1 - \bar{g}_{1c}/g)^{\beta}, \tag{7}$$

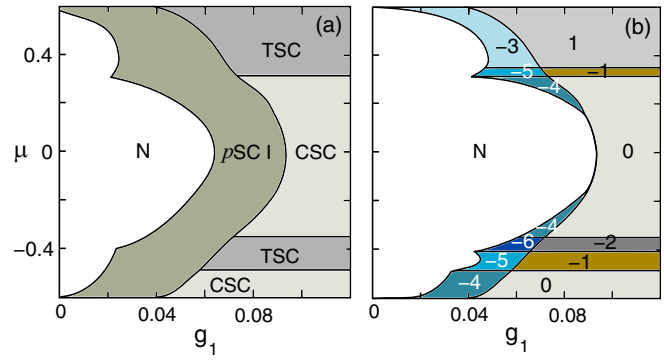

FIG. 3. Mean-field phase diagram as a function of the chemical potential μ and intraorbital pairing coupling g_1, both in eV units. The phase diagram does not depend on g_2 for $g_2 \lesssim 0.1$ eV (see Fig. 2). (a) Normal phase (N), p_x superconducting phase (pSC I), chiral $p+ip$ state (CSC), and topological $p+ip$ phase (TSC). (b) Possible topological phases in the chiral $p+ip$ channel. The integers indicate the corresponding BdG Chern number $\mathcal{N}$. For fixed g_1, the system has a sequence of topological phase transitions near the van Hove singularities of the band, where the topology of the Fermi surface changes. The blue regions correspond to the weak-coupling gapped $p+ip$ phases, which are topological. Gray and maroon regions: Strong-coupling phases. In the mean field, the gapped $p+ip$ state wins over the nonchiral p state in the strong-coupling sector.

with $\beta \approx 2.7 \pm 0.1$ for $0.2 \lesssim \mu \lesssim 0.4$ eV [see Fig. 2(c) inset]. Δ_1^C vanishes at the critical coupling $\bar{g}_{1c}$, where the system has a second-order phase transition to the normal state, indicated by the green arrows in Fig. 2. A qualitatively similar behavior is also observed in the scaling of the intraorbital p-wave gap Δ_1^p near the critical coupling $\tilde{g}_1(\mu)$ (blue arrows in Fig. 2) [33].

When μ is in the immediate vicinity of the van Hove singularities, $\bar{g}_{1c}$ abruptly drops towards zero. This singular behavior suggests a crossover to exponential scaling when the Fermi surface is nested at the van Hove singularities [33]. In that regime, the phase transition is not quantum critical. A similar behavior is also observed in the pSC I phase near the van Hove. At the saddle points, the order parameter can be broken into four patches related by the C_4 symmetry of the bands combined with odd angular momentum of the Cooper pairs. By symmetry, the free energy written in a basis of p_x and p_y pairing states is

$$\mathcal{F}(\Delta_x^p, \Delta_y^p) = \alpha\left(|\Delta_x^p|^2 + |\Delta_y^p|^2\right) + \beta\left(|\Delta_x^p|^2 + |\Delta_y^p|^2\right)^2 - \frac{\beta}{2}\left|\left(\Delta_x^p\right)^2 - \left(\Delta_y^p\right)^2\right|^2 + O(\Delta^6), \tag{8}$$

where $\alpha < 0$ in the ordered state and $\beta > 0$ [33]. The last term favors coexistence between Δ_x^p and Δ_y^p with a $\pm\pi/2$ phase difference ($p+ip$ phase), while the second one favors a nonchiral p state. The chiral and nonchiral phases are exactly degenerate at the mean-field level up to quartic-order terms in the expansion. Their degeneracy will likely be lifted by fluctuations, which will be addressed elsewhere.

In general, all the gapped chiral phases prevail over the gapless one (Δ_2^C). At small doping, the two critical couplings of the weak- and strong-coupling phases merge ($\bar{g}_{1c} = g_{1c}$)

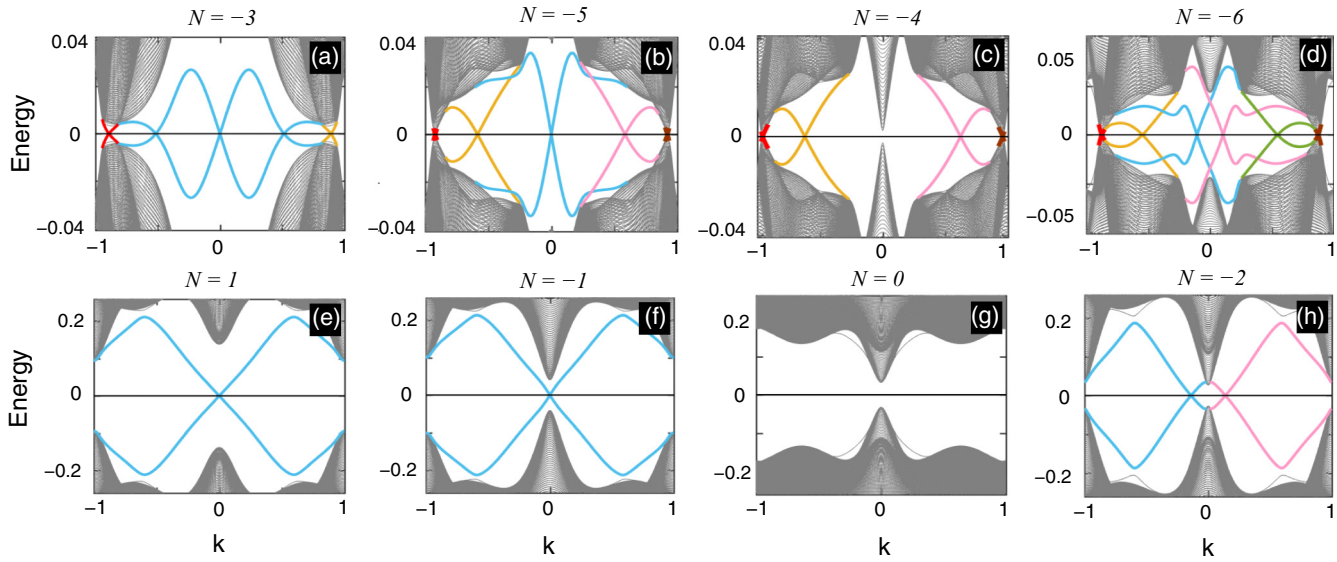

FIG. 4. Majorana edge modes in the different topological phases in the gapped $p + ip$ state. Energy units in eV. (a) BdG Chern number $\mathcal{N} = -3$ state, at $\mu = 0.44$ eV. (b) $\mathcal{N} = -5$ at $\mu = 0.33$ eV. (c) $\mathcal{N} = -4$ at $\mu = -0.49$ eV and (d) $\mathcal{N} = -6$ at $\mu = -0.38$ eV in the weak-coupling regime. The lower panels give the corresponding phases in the strong-coupling sector: (e) $\mathcal{N} = 1$ at $\mu = 0.44$ eV, (f) $\mathcal{N} = -1$ at $\mu = 0.33$ eV; (g) $\mathcal{N} = 0$ at $\mu = -0.49$ eV, which is topologically trivial and (h) $\mathcal{N} = -2$ at $\mu = -0.38$ eV. At the crossing from the weak- to strong-coupling phases, when $g = g_{1c}(\mu)$, all Chern numbers increase by 4.

below $|\mu| \lesssim 0.6t$ and the gapped phase has a first-order phase transition to the normal state at $g < g_{1c}(\mu)$ [see Fig. 3(b)].

IV. TOPOLOGICAL PHASE TRANSITIONS

In 2D, spinless superconductors with a bulk gap that breaks time-reversal symmetry belong to the C class in the tenfold classification table [34,35]. The topological number in this class is defined by the BdG Chern number $\mathcal{N}$, which corresponds to the number of chiral Majorana modes propagating along the edge [7,36].

In Fig. 3(b), we explicitly calculate the Chern number

$$\mathcal{N} = (i/2\pi) \int_{\mathrm{BZ}} d^2\mathbf{q}\, \Omega_z(\mathbf{q}) \tag{9}$$

in the gapped state as a function of μ and intraorbital coupling g_1, with $\mathbf{\Omega}(\mathbf{q}) = \nabla_{\mathbf{q}} \times \langle \psi_{n,\mathbf{q}} | \nabla_{\mathbf{q}} | \psi_{n,\mathbf{q}} \rangle$ the Berry curvature from the eigenstates of the BdG Hamiltonian at the Fermi level, $|\psi_{n,\mathbf{q}}\rangle$. By changing the chemical potential, the system shows a sequence of topological phase transitions.

In the weak-coupling phase, shown in the blue areas in Fig. 3(b), there are up to five transitions separating different topological phases with $\mathcal{N} = -4$, -5, -6, -4, -5, and -3, in the range of $-2t \leqslant \mu \leqslant 2t = 0.6$ eV. The critical values of the chemical potential where the system has a topological phase transition are close to the energy of the van Hove singularities of the band [see Fig. 1(c)] and coincide with the energies where the topology of the Fermi surface changes. At those critical values, the superconducting gap closes and the Chern number jumps by an integer number. The line $g_1 = \bar{g}_{1c}(\mu)$ separates the blue areas from the normal region through continuous phase transitions. As anticipated, when $|\mu| \lesssim 0.6t = 0.18$ eV, $\bar{g}_{1c} = g_{1c}$, and the weak-coupling phases are suppressed. The singular behavior of $\bar{g}_{1c}(\mu)$ when μ is at the van Hove is not captured by the numerics shown in Fig. 3 due to the smallness of the gap.

The solid curve separating the blue regions in Fig. 3(b) from the strong-coupling phases sets $g_{1c}(\mu)$, which describes a line of first-order phase transitions between different gapped phases. At this line, the order parameter is discontinuous [37], indicating the onset of a topological phase transition as a function of g_1 for fixed μ. In all cases, the Chern number changes across the $g_{1c}(\mu)$ line by $\Delta\mathcal{N} = 4$. Deep in the strong-coupling regime (gray and maroon regions), for fixed $g > g_{1c}(\mu = 0)$, there are six topological phase transitions separating the phases $\mathcal{N} = 0$, -1, -2, 0, -1, 1, 0 as a function of the chemical potential. The $\mathcal{N} = 0$ phases (CSC) are chiral but topologically trivial. At the wide doping window $1.27t \lesssim \mu \lesssim 2t = 0.6$ eV, the elemental chiral topological superconducting phase with $\mathcal{N} = \pm 1$, and hence a single Majorana mode, can emerge at strong coupling.

V. CHIRAL MAJORANA EDGE STATES

To explicitly verify the Chern numbers for the different phases, we calculate the edge modes of the gapped state in a two-dimensional strip geometry with edges oriented along the (1,0) direction.

The plots in Figs. 4(a)–4(d) (top row) show the evolution of the edge modes in the weak-coupling regime [$\bar{g}_{1c} < g < g_c(\mu)$] for different values of μ. The $\mathcal{N} = -3$ state shown in Fig. 4(a) has five edge modes in total, but only three modes that are topologically protected, as indicted by the three different colors. The three modes indicated in blue can be adiabatically deformed into a single zero-energy crossing at $k = 0$, and hence count as a single topologically protected mode. By decreasing the chemical potential into the contiguous $\mathcal{N} = -5$ state [Fig. 4(b)], two of those modes become topologically protected, raising the number of Majorana modes to five. By

reducing μ further into the $\mathcal{N} = -4$ state, the topology of the Fermi surface changes drastically, forming gapped pockets of charge around four Dirac nodes, indicated in Fig. 1(c). Figure 4(d) shows the edge modes of the $\mathcal{N} = -6$ state, for $\mu \lesssim -t = -0.3$ eV. The corresponding edge modes in the strong-coupling regime [$g > g_{1c}(\mu)$] with $\mathcal{N} = 1, -1, 0$, and -2 are shown in the bottom row of Figs. 4(e)–4(h).

VI. PAIRING MECHANISM

Although it is difficult to reliably predict a mechanism of superconductivity, at large doping and in the vicinity of the van Hove singularities, where the DOS is very large, both phonons and electronic interactions could be suitable candidates for a pairing mechanism. We will not discuss the phonon mechanism, since it is conventional.

Electronic mechanisms typically provide attraction when the charge susceptibility at the Fermi-surface nesting vector $\mathbf{Q}$ satisfies $\chi(\mathbf{Q}) > \chi(0)$ [38]. When the chemical potential μ is close to a van Hove singularity, the electronic bands have an energy spectrum $\epsilon(\mathbf{q}) = -\alpha q_x^2 + \beta q_y^2$ $(0 < \alpha \leqslant \beta)$, where $\mathbf{q}$ is the momentum away from the saddle point. The susceptibility in the vicinity of the singularity is logarithmic divergent, $\chi(0) = \frac{1}{2\pi^2}/\sqrt{\alpha\beta}\ln(\Lambda/\delta\mu)$, with $\delta\mu$ the deviation away from the van Hove and $\Lambda \sim t$ an ultraviolet cutoff around the saddle point [39]. At the nesting wave vector $\epsilon(\mathbf{q}+\mathbf{Q}) = -\alpha p_y^2 + \beta p_x^2$, the susceptibility is

$$\chi(\mathbf{Q}) = c/(\alpha+\beta)\ln(\Lambda/\delta\mu), \tag{10}$$

where the constant $c = \frac{1}{\pi^2}\ln\left(\sqrt{\frac{\alpha}{\beta-\alpha}} + \sqrt{\frac{\beta}{\beta-\alpha}}\right)$ is logarithmically divergent at the nesting condition $\alpha = \beta$ [40]. For the particular lattice Hamiltonian parametrization taken from Ref. [27], the fitting of the bands around the van Hove at $\mu = 0.312$ eV has $\alpha \approx 1.2$ and $\beta \approx 1.7$. That gives the ratio $\chi(\mathbf{Q})/\chi(0) \sim 1.20$, suggesting that a purely electronic mechanism of superconductivity is possible [39,41,42]. The high doping regime could in principle be reached with gating effects for CrO_2 encapsulated in an insulating substrate [43] that preserves the rotoinversion symmetry of the lattice.

ACKNOWLEDGMENTS

B.U. acknowledges K. Mullen for discussions. X.D., K.S., and B.U. acknowledge NSF CAREER Grant No. DMR-1352604 for partial support.

[1] Y. S. Dedkov, M. Fonine, C. König, U. Rüdiger, and G. Güntherodt, Appl. Phys. Lett. **80**, 4181 (2002).
[2] R. J. Soulen Jr., J. M. Byers, M. S. Osofsky, B. Nadgorny, T. Ambrose, S. F. Cheng, P. R. Broussard, C. T. Tanaka, J. Nowak, J. S. Moodera, A. Barry, and J. M. D. Coey, Science **282**, 85 (1998).
[3] W. E. Pickett, Phys. Rev. Lett. **77**, 3185 (1996).
[4] A. P. Mackenzie and Y. Maeno, Rev. Mod. Phys. **75**, 657 (2003).
[5] C. Kallin and J. Berlinsky, Rep. Prog. Phys. **79**, 54502 (2016).
[6] Y. Maeno, S. Kittaka, T. Nomura, S. Yonezawa, and K. Ishida, J. Phys. Soc. Jpn. **81**, 011009 (2012).
[7] N. Read and D. Green, Phys. Rev. B **61**, 10267 (2000).
[8] X.-L. Qi, T. L. Hughes, S. Raghu, and S.-C. Zhang, Phys. Rev. Lett. **102**, 187001 (2009).
[9] X.-L. Qi, and S.-C. Zhang, Rev. Mod. Phys. **83**, 1057 (2011).
[10] J. Alicea, Rep. Prog. Phys. **75**, 076501 (2012).
[11] P. A. Lee, Science **346**, 545 (2014).
[12] M. Sato and Y. Ando, Rep. Prog. Phys. **80**, 076501 (2017).
[13] S. B. Chung, H. Bluhm, and E.-A. Kim, Phys. Rev. Lett. **99**, 197002 (2007).
[14] J. Jang, D. G. Ferguson, V. Vakaryuk, R. Budakian, S. B. Chung, P. M. Goldbart, and Y. Maeno, Science **331**, 186 (2011).
[15] R. Jackiw and P. Rossi, Nucl. Phys. B **190**, 681 (1981).
[16] J.-P. Xu, M.-X. Wang, Z. L. Liu, J.-F. Ge, X. Yang, C. Liu, Z. A. Xu, D. Guan, C. L. Gao, D. Qian, Y. Liu, Q.-H. Wang, F.-C. Zhang, Q.-K. Xue, and J.-F. Jia, Phys. Rev. Lett. **114**, 017001 (2015).
[17] L. Fu and C. L. Kane, Phys. Rev. Lett. **100**, 096407 (2008).
[18] A. R. Akhmerov, J. Nilsson, and C. W. J. Beenakker, Phys. Rev. Lett. **102**, 216404 (2009).
[19] L. Fu and C. L. Kane, Phys. Rev. Lett. **102**, 216403 (2009).
[20] R. M. Lutchyn, J. D. Sau, and S. Das Sarma, Phys. Rev. Lett. **105**, 077001 (2010).
[21] S. B. Chung, H.-J. Zhang, X.-L. Qi, and S.-C. Zhang, Phys. Rev. B **84**, 060510(R) (2011).
[22] J. Li, T. Neupert, Z. J. Wang, A. H. MacDonald, A. Yazdani, and B. A. Bernevig, Nat. Commun. **7**, 12297 (2016).
[23] X.-L. Qi, T. L. Hughes, and S.-C. Zhang, Phys. Rev. B **82**, 184516 (2010).
[24] Q. L. He, L. Pan, A. L. Stern, E. Burks, X. Che, G. Yin, J. Wang, B. Lian, Q. Zhou, E. S. Choi, K. Murata, X. Kou, T. Nie, Q. Shao, Y. Fan, S.-C. Zhang, K. Liu, J. Xia, and K. L. Wang, Science **357**, 294 (2017).
[25] K. Schwarz, J. Phys. F: Met. Phys. **16**, L211 (1986).
[26] M. I. Katsnelson, V. Yu. Irkhin, L. Chioncel, A. I. Lichtenstein, and R. A. de Groot, Rev. Mod. Phys. **80**, 315 (2008).
[27] T. Cai, X. Li, F. Wang, S. Ju, J. Feng, and C.-D. Gong, Nano Lett. **15**, 6434 (2015).
[28] While $t_4 = 0$ by the symmetry of the crystal, spin-orbit coupling effects lead to a finite imaginary $t_4 = it/8 \approx \pm(i)0.036$ eV. See Ref. [27]. This term opens a small gap of ∼4 meV at the Dirac nodes.
[29] N. Furukawa, T. M. Rice, and M. Salmhofer, Phys. Rev. Lett. **81**, 3195 (1998).
[30] R. Nandkishore, L. S. Levitov, and A. V. Chubukov, Nat. Phys. **8**, 158 (2012).
[31] M. L. Kiesel, C. Platt, W. Hanke, D. A. Abanin, and R. Thomale, Phys. Rev. B **86**, 020507(R) (2012).
[32] The p_y state is also allowed by symmetry. All nonchiral combinations of p_x and p_y pairing symmetry have higher energy and are subdominant.
[33] See Supplemental Material at http://link.aps.org/supplemental/10.1103/PhysRevB.99.104503 for a more detailed analysis of the quantum critical scaling and for a symmetry analysis.
[34] A. P. Schnyder, S. Ryu, A. Furusaki, and A. W. W. Ludwig, Phys. Rev. B **78**, 195125 (2008).

[35] S. Ryu, A. Schnyder, A. Furusaki, and A. Ludwig, New J. Phys. **12**, 65010 (2010).
[36] D. J. Thouless, M. Kohmoto, M. P. Nightingale, and M. den Nijs, Phys. Rev. Lett. **49**, 405 (1982).
[37] The spectral gap does not close along the line of first-order topological phase transitions. The gap closes, however, if Δ_1 is virtually changed as a continuous parameter connecting two topologically distinct ground states.
[38] W. Kohn and J. M. Luttinger, Phys. Rev. Lett. **15**, 524 (1965).
[39] J. Gonzalez, Phys. Rev. B **78**, 205431 (2008).
[40] P. C. Pattnaik, C. L. Kane, D. M. Newns, and C. C. Tsuei, Phys. Rev. B **45**, 5714 (1992).
[41] F. Guinea and B. Uchoa, Phys. Rev. B **86**, 134521 (2012).
[42] This mechanism does not in principle discard the possibility of particle-hole instabilities. In the square lattice, they are known to be subleading to superconductivity in the singlet channel. See Ref. [29].
[43] A. S. Mayorov, R. V. Gorbachev, S. V. Morozov, L. Britnell, R. Jalil, L. A. Ponomarenko, P. Blake, K. S. Novoselov, K. Watanabe, T. Taniguchi, and A. K. Geim, Nano Lett. **11**, 2396 (2011).